AGU PUBLICATIONS

JGR

Journal of Geophysical Research: Atmospheres

RESEARCH ARTICLE
10.1002/2017JD027171

Key Points:
- The CIO mode is a natural ocean-atmosphere coupled mode, but it is not well captured in CESM
- Weak meridional gradient of large-scale zonal winds is a main reason for the poor simulation of the CIO mode in CESM
- A better CIO mode simulation benefits the Indian monsoon simulation, and the CIO mode can be a coupled metric for evaluating climate models

Supporting Information:
- Supporting Information S1

Correspondence to:
L. Zhou,
zhoulei1588@sjtu.edu.cn

Citation:
Zhou, L., Murtugudde, R., Neale, R. B., & Jochum, M. (2018). Simulation of the Central Indian Ocean mode in CESM: Implications for the Indian summer monsoon system. *Journal of Geophysical Research: Atmospheres*, *123*, 58–72. https://doi.org/10.1002/2017JD027171

Received 20 MAY 2017
Accepted 5 DEC 2017
Accepted article online 13 DEC 2017
Published online 4 JAN 2018

©2017. American Geophysical Union. All Rights Reserved.

Simulation of the Central Indian Ocean Mode in CESM: Implications for the Indian Summer Monsoon System

Lei Zhou[1,2,3], Raghu Murtugudde[4], Richard B. Neale[5], and Markus Jochum[6]

[1]Institute of Oceanography, Shanghai Jiao Tong University, Shanghai, China, [2]Laboratory for Regional Oceanography and Numerical Modeling, Qingdao National Laboratory for Marine Science and Technology, Qingdao, China, [3]State Key Laboratory of Satellite Ocean Environment Dynamics, Second Institute of Oceanography, Hangzhou, China, [4]Earth System Science Interdisciplinary Center, University of Maryland, College Park, MD, USA, [5]National Center for Atmospheric Research, Boulder, CO, USA, [6]Niels Bohr Institute, University of Copenhagen, Copenhagen, Denmark

Abstract The simulation of the Indian summer monsoon and its pronounced intraseasonal component in a modern climate model remains a significant challenge. Recently, using observations and reanalysis products, the central Indian Ocean (CIO) mode was found to be a natural mode in the ocean-atmosphere coupled system and also shown to have a close mechanistic connection with the monsoon intraseasonal oscillation (MISO). In this study, the simulation of the actual CIO mode in historical Community Earth System Model (CESM) outputs is assessed by comparing with observations and reanalysis products. The simulation of the Madden-Julian Oscillation, a major component of tropical intraseasonal variabilities (ISVs), is satisfactory. However, the CIO mode is not well captured in any of the CESM simulations considered here. The force and response relationship between the atmosphere and the ocean associated with the CIO mode in CESM is opposite to that in nature. The simulated meridional gradient of large-scale zonal winds is too weak, which precludes the necessary energy conversion from the mean state to the ISVs and cuts off the energy source to MISO in CESM. The inability of CESM to reproduce the CIO mode seen clearly in nature highlights the CIO mode as a new dynamical framework for diagnosing the deficiencies in Indian summer monsoon simulation in climate models. The CIO mode is a coupled metric for evaluating climate models and may be a better indicator of a model's skill to accurately capture the tropical multiscale interactions over subseasonal to interannual timescales.

1. Introduction

Monsoon intraseasonal oscillations (MISO) are most pronounced during the Indian summer monsoon, accounting for about 60% of total precipitation variance over the Bay of Bengal (BoB) (Goswami, 2005; Waliser, 2006). Considering the high correlations between precipitation variability over the BoB and the Indian subcontinent, and the larger Asian monsoon in general, any insights into the intraseasonal variabilities (ISVs) over the BoB will enhance our understanding of the Asian monsoons, with implications for the African and Australian monsoons and the monsoon-El Niño–Southern Oscillation (ENSO) interactions as a whole (Li & Zeng, 2002; McPhaden et al., 2009; Pottapinjara et al., 2014; Webster et al., 1998). In addition, a better understanding of MISO also has an obvious scientific and socioeconomic significance for the livelihood of billions of people living on the rim of the Indian Ocean. To date, the predictability of monsoon rainfall remains low (Wang et al., 2015), which is attributable to the much-debated relationship between MISO and the major intrinsic climate modes, such as ENSO (e.g., Gill et al., 2015; Kumar et al., 2006) and the Indian Ocean Dipole-Zonal Mode (IODZM) (e.g., Ashok et al., 2001; Kripalani & Kumar, 2004; Murtugudde & Busalacchi, 1999; Murtugudde et al., 2000). Recently, a central Indian Ocean (CIO) mode, which is defined using a combination of intraseasonal sea surface temperature (SST) anomalies and intraseasonal low-level wind anomalies over the Indian Ocean, was found to have a close relation with monsoonal rainfall (Zhou et al., 2017b). For the observed CIO mode, the warm intraseasonal SST anomalies are coherent with an anticyclone and the associated downdraft in the atmosphere over the central Indian Ocean. Meanwhile, the easterly wind shear in the vertical is enhanced, which favors the northward propagation of ISVs. As a result, the diagnoses using observations and reanalysis products indicate that the coupling between the dynamic and thermodynamic fields results in a high correlation between the CIO mode index and the MISO. In addition, the barotropic instability was found to be responsible for the seasonal and interannual variabilities of the CIO mode

(Zhou et al., 2017a). In particular, the interannual variabilities in MISO have a high consistency with those of the CIO mode, but not with those of ENSO or IODZM. The CIO mode does not have a significant linear correlation with ENSO or IODZM, either. Therefore, besides current understanding of the impacts of ENSO and IODZM on MISO, it can be deduced that the CIO mode provides an independent and useful information to advance our understanding of MISO at various timescales.

Generally, there are two major components of ISVs over the Indo-Pacific region (Wang & Rui, 1990). One is the eastward propagating component, prevalent during boreal winter and is commonly known as the Madden-Julian Oscillation (MJO) (e.g., Madden & Julian, 1994; Zhang, 2005). The other is the MISO, which mainly propagates northward during Indian summer monsoon (e.g., Lau et al., 2012; Waliser, 2006). The simulation of ISVs continues to be a major remaining challenge to weather and climate modeling, predictions, and projections. For MJOs, several multimodel comparisons have been conducted (e.g., Kim et al., 2009; Lin et al., 2006; Slingo et al., 1996; Waliser, Jin, et al., 2003). Although different models were examined in different comparison projects, a common conclusion is that the MJO simulation is poor, but recently improving. With the coordinated efforts, especially the intensive in situ observation projects such as the Cooperative Indian Ocean Experiment on Intraseasonal Variability and the Dynamics of the MJO (Yoneyama et al., 2013), the MJO simulations have significantly improved. In particular, CESM and its previous versions of Community Climate System Model (CCSM) have demonstrated an ability to reproduce the MJO (Boyle et al., 2015; Li et al., 2016; Subramanian et al., 2011; Zhou, Neale, et al., 2012). Many studies have also been dedicated to the MISO simulation (Ajayamohan et al., 2014; Lin et al., 2008; Sperber & Annamalai, 2008). With the intercomparisons of many atmospheric general circulation models, Waliser, Lau, et al. (2003) concluded that most models lack coherent ISVs during monsoon seasons, especially over the equatorial Indian Ocean. Using the National Centers for Environmental Prediction (NCEP) Climate Forecast System model (version 2), Goswami et al. (2014) also showed a bias in MISO simulation due to the lack of coherence between convection and SST anomalies over the tropical Indian Ocean. For CCSM, the monsoon simulation was summarized in Meehl et al. (2006) and Meehl et al. (2012), but a reasonable MISO simulation was absent. In an examination of five different CESM experiments, Li et al. (2016) indicated that the eastward propagating MJO was well simulated but the northward propagating MISO apparently deviated from reality. Hence, in contrast to MJO simulations, there is still much progress to be made in improving MISO simulations in climate models.

Various possible avenues to improve MISO simulations in climate models, including CESM, have been proposed and examined. Using a coupled model instead of an atmosphere-only model has been found to be important for process understanding, since the two-way interactions between the ocean and the atmosphere are important for the evolution and lifecycle of MISO (e.g., Fu et al., 2007; Fu & Wang, 2004; Kemball-Cook et al., 2002). A better representation of the mean state (Kemball-Cook et al., 2002) and a more comprehensive model physics in computing surface heat flux (Lin et al., 2005) were both shown to improve the MISO simulation. In addition, the inclusion of key dynamical processes in a climate model is another possible way to improve MISO simulations. The CIO mode proposed in Zhou et al. (2017b) should be a good candidate for this avenue, since it is shown to capture the coupled air-sea interactions associated with MISO based on the dynamical and statistical analyses using observations and reanalysis products.

The actual structures and features of the CIO mode have been reported in Zhou et al. (2017a, 2017b). In this study, the simulations of CIO mode are examined against the observations. Due to the close relation between the CIO mode and MISO in nature, such examinations can shed light on ways of more dynamically diagnosing MISO and Indian summer monsoon simulations. This is the motivation for this paper. For the rest of this paper, model configurations and daily historical CESM outputs used in this study are introduced in section 2. The assessments of the CIO mode simulations on various timescales are shown in section 3. The conclusions and discussion are presented in section 4.

2. Historical CESM Outputs

In this study, daily historical outputs are used from the CESM Large Ensemble Project (referred to as LEN hereafter) and the CESM Whole Atmosphere Community Climate Model (referred to as WACCM hereafter) historical runs.

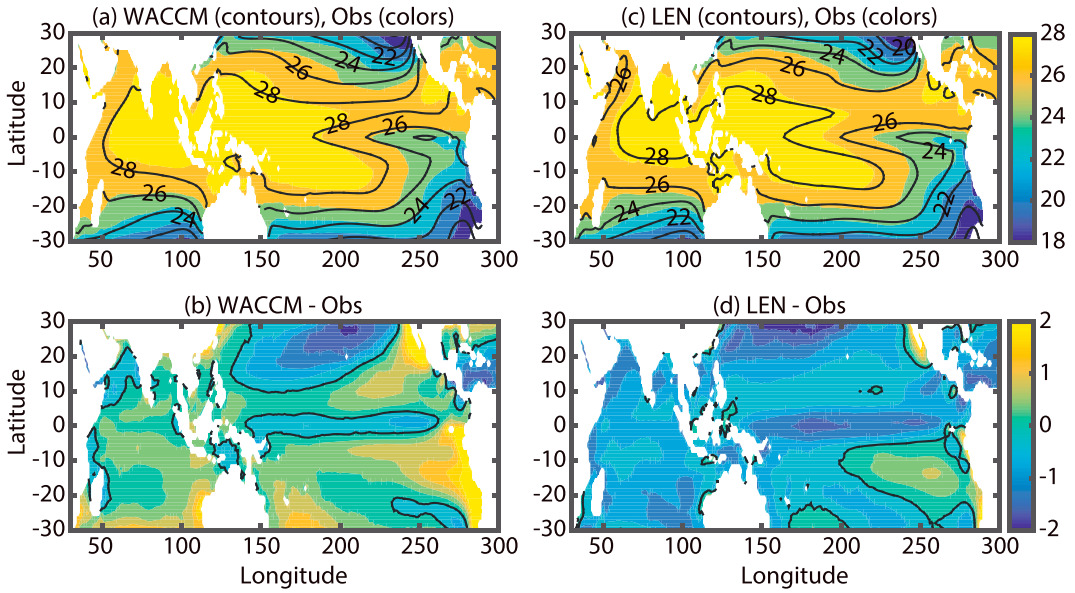

Figure 1. (a) Mean SST averaged from 1986 to 2005 in the historical CESM WACCM (contours) and in observations (colors). (b) SST differences between CESM WACCM and observations. The black contours mark zero of the SST differences. (c and d) Same as Figures 1a and 1b but for the ensemble mean of 30 CEMS LEN members. The unit is °C.

LEN is designed in order to be able to examine the internal climate variability of the CESM in a systematic way. A comprehensive overview of LEN is provided in Kay et al. (2015). Thirty CESM ensemble members are created using the same model and the same external forcing. The differences among the ensemble members only reside in the small round-off perturbations in the initial atmospheric conditions. The historical runs are conducted from 1920 to 2005, branching of the same single simulations that ran from 1850 to 1920. The horizontal resolution for the atmosphere is approximately 0.95° latitude × 1.25° longitude, and the average horizontal resolution for the ocean is approximately 0.27° latitude × 1.125° longitude, with finer resolution close to the equator. The details about WACCM are presented in Marsh et al. (2013). WACCM provides a more realistic representation of stratospheric processes as well as the interactions between the troposphere and the stratosphere, and as a consequence has a superior simulation of the quasi-biennial oscillation (QBO) compared to LEN. The atmosphere component of WACCM extends up to 1 hPa and includes fully interactive chemistry. The historical WACCM is also conducted from 1850 to 2005. In WACCM, the horizontal resolution for the atmosphere is approximately 1.9° latitude × 2.5° longitude, and the horizontal resolution for the ocean remains approximately 0.27° latitude × 1.125° longitude. The two sets of CESM outputs are selected because they have daily outputs (which are required for resolving ISVs) for both atmospheric and oceanic variables. In this study, we mainly focus on the common performance of the CIO mode simulations in CESM. We do not fully examine the differences among the model runs, which are likely to be attributable to different and special model configurations (such as the interactions between the troposphere and the stratosphere in WACCM). The internal variabilities of the CIO mode simulations in different model runs are of great scientific importance, which will be studied in the future.

For the assessment of CESM simulations, atmospheric variables are obtained from the daily NCEP-U.S. Department of Energy Reanalysis 2 (NCEPR2) (Kanamitsu et al., 2002). Precipitation is from the standard pentad Climate Prediction Center Merged Analysis of Precipitation (CMAP) (Xie & Arkin, 1997). SST data are from the NOAA 1/4° daily Optimum Interpolation SST (OISST) (Reynolds et al., 2007), and the outgoing longwave radiation (OLR) is obtained from NOAA polar-orbiting series of satellites (Liebmann & Smith, 1996). The properties of the CIO mode are presented in details in Zhou et al. (2017a, 2017b), which remain robust even when data from different sources are used.

Daily CESM outputs, observations, and NCEPR2 reanalysis from 1986 to 2005, 20 years in all, are used for the diagnostics. All intraseasonal variabilities are obtained with a Butterworth band-pass filter between 20 days and 100 days.

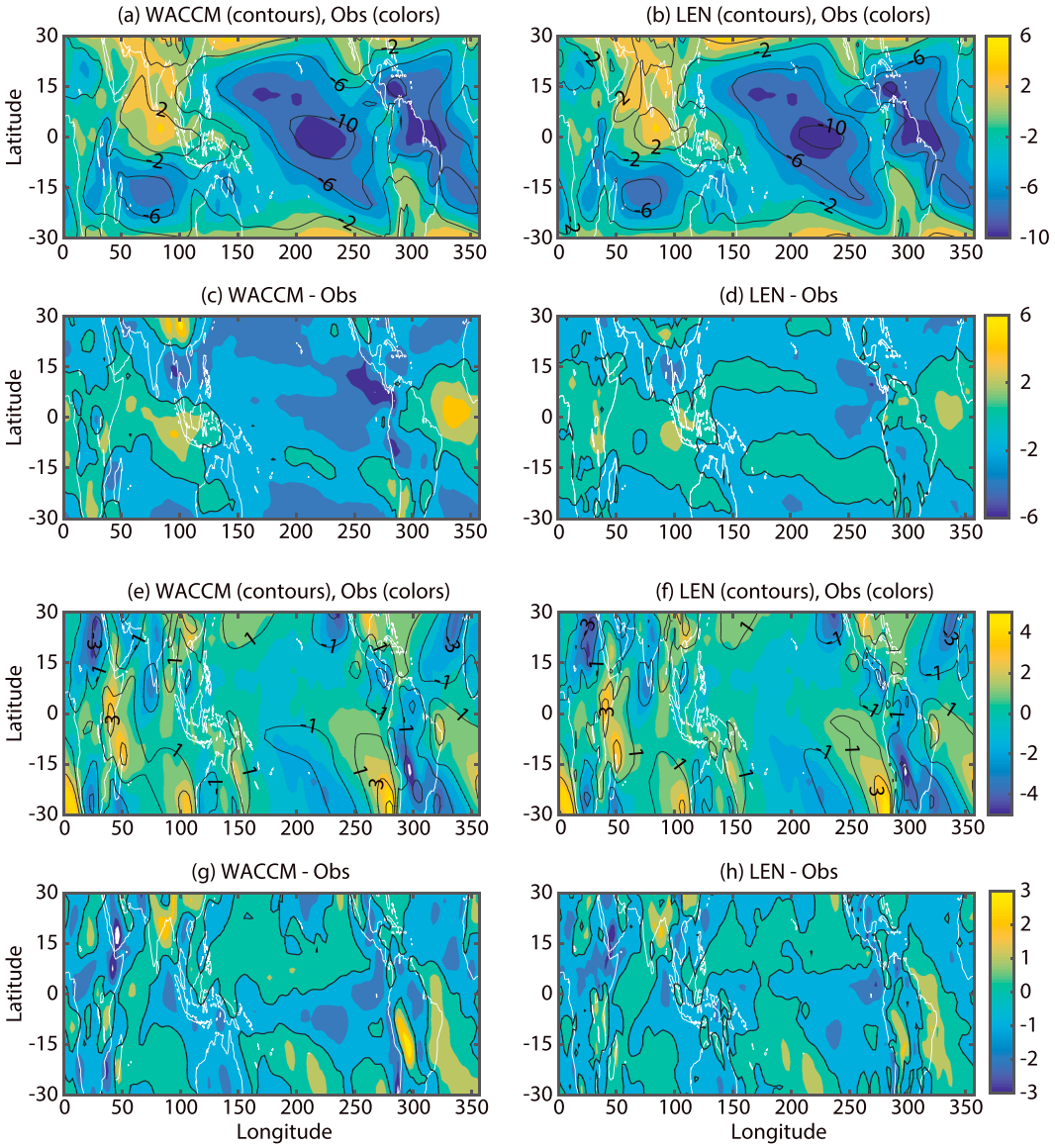

Figure 2. (a) Mean zonal winds at 850 hPa averaged from 1986 to 2005 in CESM WACCM (contours) and in the NCEPR2 reanalysis (colors). (c) Differences in zonal winds at 850 hPa between CESM WACCM and observations. The black contours mark zero of the zonal wind differences. (b and d) Same as Figures 2a and 2c but for the ensemble mean of 30 CEMS LEN members. (e–h) Same as Figures 2a–2dbut for the meridional winds at 850 hPa. The unit is m s^{-1}.

3. Results

3.1. Simulation of the Mean Climate State and Monsoon

The simulated mean SST and mean winds at 850 hPa for WACCM and for the 30 LEN ensemble members are shown in Figures 1 and 2. The differences between the mean simulated SST and observations are generally smaller than 2°C (Figure 1). Especially, in the area of interest from the Indian Ocean to the western Pacific, the simulation errors are mostly smaller than 0.5°C. The differences in the zonal winds at 850 hPa are generally smaller than 2 m s^{-1} over the Indo-Pacific region (Figures 2a–2d). In addition, the weak westerly winds over the equatorial Indian Ocean are captured in both outputs, which are significant improvements over previous model versions (e.g., CCSM3). Such improvement was shown to benefit the MJO simulation (Zhou, Neale, et al., 2012). The meridional winds at 850 hPa also agree with reanalysis products (Figures 2e–2h). Over the Indo-Pacific region, large bias occurs along the Somali coast. The ensemble mean precipitation of LEN are compared with the CMAP rainfall in Figure 3 (rainfall is not stored in WACCM). Simulated rainfall is greater

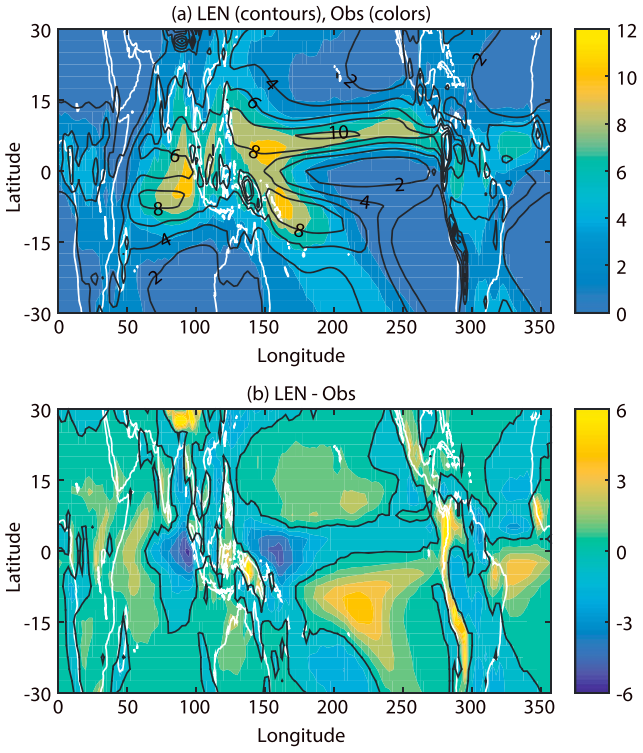

Figure 3. (a) Ensemble mean precipitation of 30 CEMS LEN members averaged from 1986 to 2005 (contours) and from CMAP (colors). (b) Differences in precipitation between LEN ensemble mean and the reanalysis. The black contours mark zero of the precipitation differences. The unit is mm d^{-1}.

over the Indian subcontinent and the western Indian Ocean than over the BoB and the Indo-China Peninsula, which is probably attributable to the weaker simulated summer monsoon (shown below). Differences do exist between WACCM and LEN, which should be attributable to different model configurations. This is also possibly due to the many members used in LEN and only a single member used in WACCM. Overall, most observed mean states are captured by both CESM products. Nevertheless, the mean state simulations are far from perfect. The mean SST biases in the West Pacific impact atmospheric variabilities as surface latent heat fluxes are lower and the low-level zonal wind profiles are not favorable for a growing MJO even if it is initialized. Large biases also exist in the Indian Ocean in LEN; for example, the eastward propagation of simulated MJO is worse in boreal winter than in boreal summer. Actually, as shown below, the poor CIO mode simulation and the weak simulated Indian summer monsoon are attributable to the bias in the large-scale simulations.

Since the CIO mode is closely related to the Indian summer monsoon, we further evaluate the Indian summer monsoon in CESM. The Indian summer monsoon can be represented by the daily tropospheric temperature (TT) index created by Goswami and Xavier (2005), which is the difference of the vertical mean temperature between 700 and 300 hPa, averaged within a northern box (35°N–10°N, 30°E–110°E) and a southern box (10°N–15°S, 30°E–110°E). During the Indian summer monsoon, the heating center jumps from the tropical Indian Ocean to the subtropics (Wu & Zhang, 1998; Zhou & Murtugudde, 2014), and the TT index changes from negative to positive. Conversely, when the Indian summer monsoon retreats, the heat source returns to the tropics and the TT index becomes negative again. The TT indices calculated with the NCEPR2 reanalysis and WACCM outputs are compared in Figure 4a. For LEN, since the air temperatures are not stored at all pressure levels, the TT index cannot be explicitly calculated. The TT index during the non-Indian summer monsoon period (negative phase) is consistent between the NCEPR2 reanalysis and the simulation (Figure 4a). However, the simulated TT index during the Indian summer monsoon is only slightly positive and much weaker than it is in the reanalysis, which indicates that the simulated Indian summer monsoon is much weaker in CESM. The weaker simulated monsoon can also be seen from the comparison between the ensemble mean precipitation in LEN and the CMAP rainfall (Figure 4b). In addition, the simulated MISO is weaker than it is in NCEPR2 reanalysis, which remains a persistent problem for most climate models. Since the tropics are the major energy source region for the subtropical ISVs during Indian summer monsoon, it can be reasonably assumed that the energy transfer from the tropics to the subtropics is not strong enough in CESM. As shown in Zhou et al. (2017b), the CIO mode controls the propagation direction of ISVs originating from the western Indian Ocean; that is, the positive CIO mode enhances the easterly wind shear in tropics and creates an environment favorable for the northward propagating MISO. Therefore, there are likely to be some problems in the CIO mode simulation, which are discussed in more detail below.

3.2. MJO Simulation in CESM

Before examining the CIO mode simulation, the MJO simulation is evaluated, since the MJO is a major component of the ISVs. The Wheeler-Hendon (WH) index (Wheeler & Hendon, 2004) and the corresponding multivariate EOF modes are used to diagnose the simulated MJO. The zonal winds at 850 hPa and 200 hPa are projected onto the EOF modes defined in Wheeler and Hendon (2004), and coefficients of the projections are referred to as the simulated RMM1 and RMM2 hereafter by analogy with the terms used in Wheeler and Hendon (2004). Since the WH index is a real-time index, projecting data onto the spatial patterns of MJO modes is a standard application of the index. The cross correlations between the simulated RMM1 and itself, and between simulated RMM1 and RMM2, are shown in Figure 5. The results for WACCM and

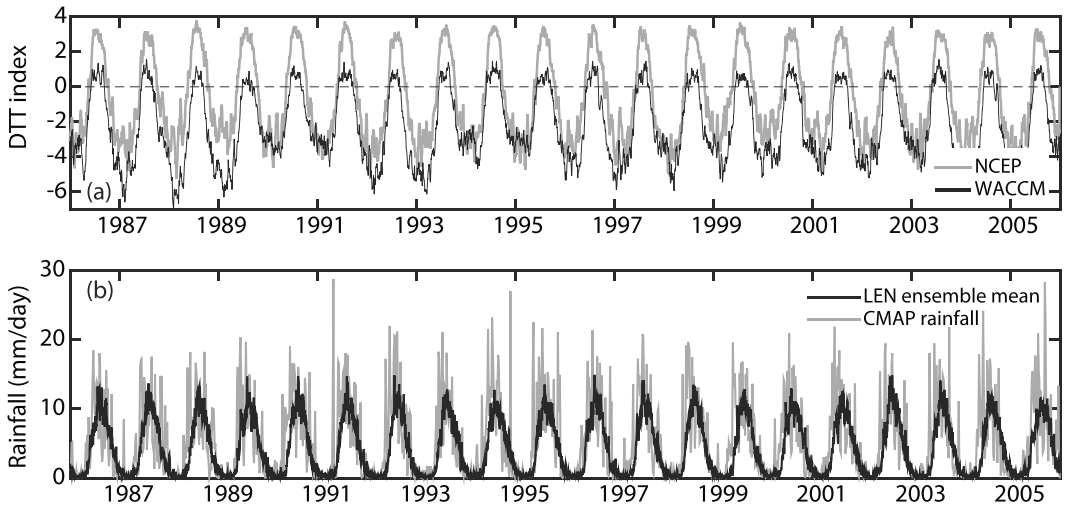

Figure 4. (a) TT index calculated with NCEPR2 reanalysis and WACCM outputs, from 1986 to 2005. (b) Mean precipitation within 85°E–95°E and 15°N–20°N, where precipitation variances are large. The black line is for the LEN ensemble mean, and the gray line is for CMAP. The unit is mm d^{-1}.

each LEN ensemble member are very similar, and all are similar to the cross correlations obtained with observations and reanalysis as shown in Wheeler and Hendon (2004) (Figure 5, thin black solid and dashed lines). Hence, the period and the coherent structure of the simulated MJO are captured adequately, which is consistent with previous reports that the CESM has a reasonable ability to simulate the MJO (Li et al., 2016; Subramanian et al., 2011; Zhou, Neale, et al., 2012). The composite of intraseasonal zonal winds at 850 hPa and intraseasonal precipitation of the eight MJO phases from LEN ensemble mean, which are defined with the two simulated RMMs, are shown in Figure 6. The phase composite of intraseasonal zonal winds from WACCM are very similar to Figure 6; hence, they are not shown. The eastward propagation of the MJO is largely reproduced, which confirms that the MJO simulation in both CESM products is acceptable. It is also obvious that the eastward propagation of the simulated zonal winds is better than that of the simulated precipitation, which is consistent with the fact that the simulation of intraseasonal rainfall is more challenging. Of course, the MJO simulation in CESM is not perfect yet. Some detailed MJO features in simulations require further improvement; for example, the MJO period tends to be a little longer and the eastward-westward power ratio of the intraseasonal spectral peaks is smaller in CESM simulations (not shown; Li et al., 2016; Waliser et al., 2009). In addition, WACCM lies slightly outside the spread of LEN values, which implies the role of QBO in modulating the MJO properties (Son et al., 2017; Weare et al., 2012). The detailed discussion on the relationship between the stratosphere and the MJO is beyond the scope of this study.

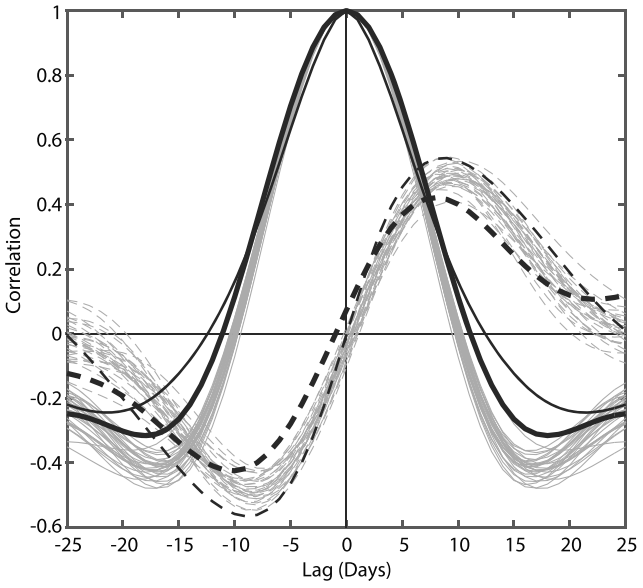

Figure 5. Cross correlation between RMM1 and itself (black lines), and between RMM1 and RMM2 (dashed lines). The thick black lines are obtained with WACCM outputs, and the gray lines are obtained with the LEN ensemble members. The thin black lines are the ones obtained with the RMM indices created by Wheeler and Hendon (2004).

3.3. Evaluation of Simulated CIO Mode: EOF Analysis

The CIO mode is captured with the first EOF mode of combined daily intraseasonal SST anomalies and daily intraseasonal zonal wind anomalies at 850 hPa in various data sets. For example, the CIO mode obtained with NCEPR2 and OISST from 1986 to 2005 is shown in Figure 7c. Such mode pattern is not sensitive to different reanalysis products or different time periods (not shown). The domain for the EOF analysis is from 40°E to 120°E and from 20°N to 20°S. The intraseasonal anomalies are obtained with a band-pass filter between 20 days and 100 days. The first EOF modes obtained from WACCM and the ensemble mean of LEN are shown in Figures 7a and 7b. The first EOF mode

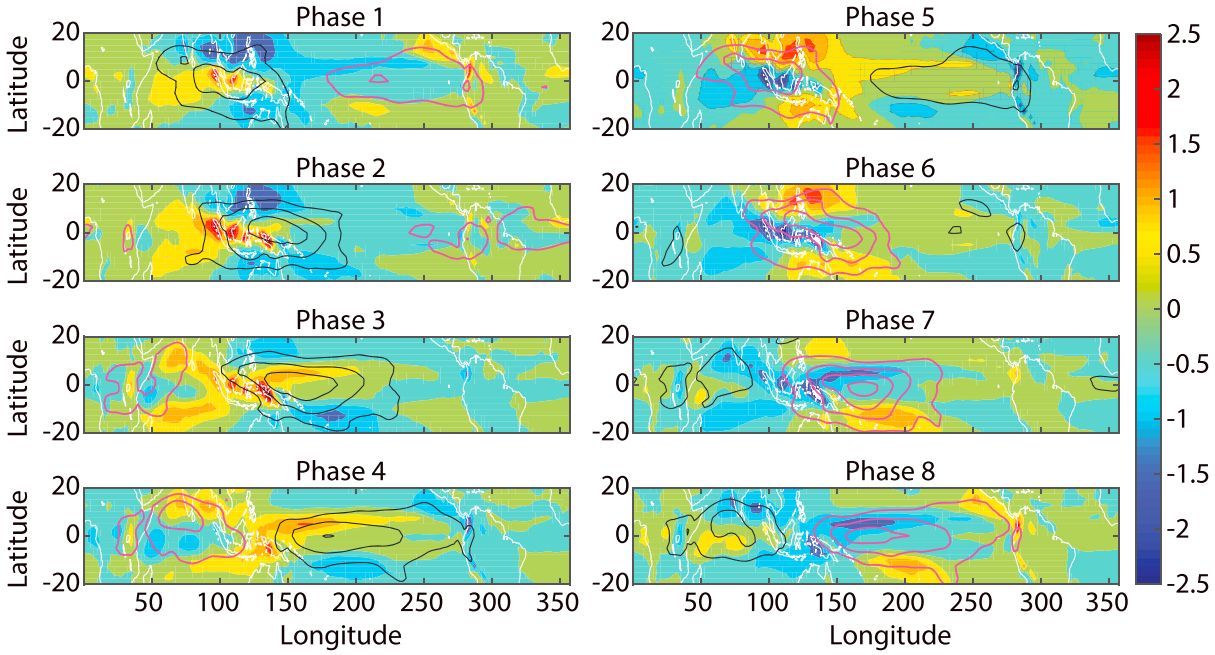

Figure 6. Phase composites of intraseasonal wind anomalies at 850 hPa in LEN (contours) and intraseasonal precipitation (colors). The purple contours are for westerly anomalies, and the black contours are for easterly anomalies. The unit for rainfall anomalies is mm d^{-1}. Contours start from ±1 m s^{-1} with an interval of 1 m s^{-1}. The eight phases are defined with the simulated RMM index for each LEN ensemble member, following Wheeler and Hendon (2004). All results shown are for the ensemble mean of 30 LEN members.

obtained from WACCM (LEN ensemble mean) explains 12.7% (11.1%) of total variance, which is significantly larger than the explained variance of 10.63% (8.8%) of the corresponding second EOF mode. In addition, the second- and high-order EOF modes in CESM are examined (not shown), and they do not resemble the actual CIO mode pattern shown in Figure 7c. It is possible that the actual CIO mode is split among multiple EOF modes. However, in CESM simulations, the observed CIO mode pattern is not discerned in any individual EOF mode. Therefore, the simulations do not reproduce the CIO mode as seen in nature. Comparing the first EOF mode in simulations (which explain the largest variance) to the mode obtained with observations and the NCEPR2 reanalysis (Figure 7c), one can see that the simulated node of positive SST anomalies shifts to the northern hemisphere. A distinct difference resides in the zonal wind mode. Easterly wind anomalies dominate the zonal wind mode. Westerly wind anomalies, which in reality are around 10°N, are barely evident in either simulation. As a result, the anticyclonic anomaly in the low-level wind mode (Figure 7c) is missing in CESM and the cyclonic structure in CESM (Figures 7a and 7b) is opposite to that in nature (Figure 7c). Fundamentally, the relation between the SST anomalies and the cyclonic anomalies in the lower troposphere indicates the force and response relation between the ocean and the atmosphere. In the CIO mode (Figure 7c), the structure of an anticyclone overlying the warm SST anomalies indicates that the atmosphere plays an active role in the ocean-atmosphere interaction (Peña, Kalnay, & Cai, 2003; Xi et al., 2015). In contrast, the structure of a cyclone over the warm SST anomalies implies that the ocean drives the atmosphere. The simplified theory from Peña et al. (2003) is suitable for diagnosing dynamical feedback between the atmosphere and ocean but may not work well for thermodynamic processes. Nevertheless, the mismatch between the simulations and observations reveals the inadequacy of the ocean-atmosphere coupling in CESM simulations, which is a typical shortcoming of monsoon simulations as emphasized by many previous studies (such as Meehl et al., 2012, and Goswami et al., 2014).

The CIO mode demonstrates a high correlation between the CIO mode index and the intraseasonal precipitation in the monsoon region during the Indian summer monsoon (Zhou et al., 2017b). Using the observations and reanalysis, high positive correlations are found over the northern BoB and they are much larger than the correlations between the Indian summer monsoon rainfall and the indices for ENSO or IODZM (not shown). We believe that the high correlation between the CIO mode index and the intraseasonal rainfall is an important and mechanistically useful property of the CIO mode and its index, which indicates a close

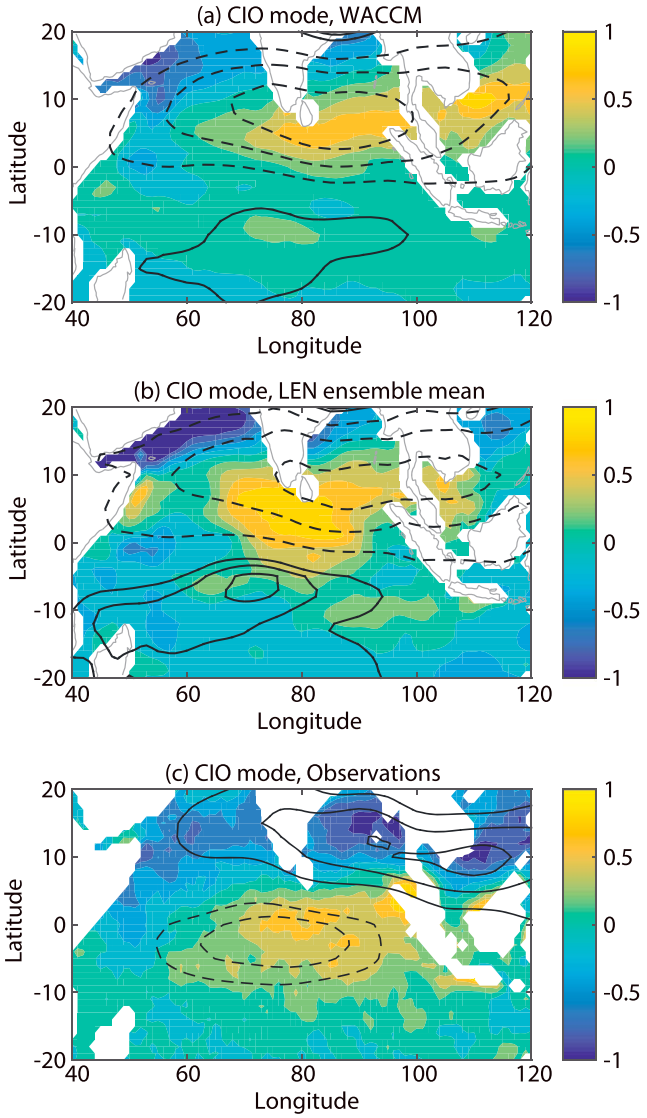

Figure 7. Comparison of the CIO mode patterns obtained by applying the EOF analysis to the (a) WACCM outputs, (b) mean LEN ensembles, and the (c) reanalysis products. The colors denote the SST nodes, reddish for positive and bluish for negative. The contours denote the zonal wind nodes, the solid contours for positive (westerly winds) and the dashed contours for negative (easterly winds). All modes are normalized, so that the maximum of the SST mode is 1. For Figures 7a and 7b, the dashed contours start from −0.5 with and interval of 0.5 and the solid contours start from 0.2 with an interval of 0.2. For Figure 7c, the dashed contours start from −0.3 with an interval of 0.3 and the solid contours start from 0.5 with an interval of 0.5. The first combined EOF mode explains 12.7% of total variance for Figure 7a, 11.1% for Figure 7b, and 13.1% for Figure 7c. EOF analysis is performed with reanalysis and simulation outputs from 1986 to 2005, but the patterns and principals of EOF modes are not sensitive to the data length.

relation between the CIO mode and the Indian summer monsoon, although precipitation has higher variance at smaller spatial and temporal scales compared to the large-scale TT index. The same correlations between the simulated CIO mode index and the Indian summer monsoon rainfall in the LEN ensemble #1 (which is taken as an example and the results for other ensemble members are qualitatively similar) are shown in Figure 8a. Although the correlation coefficients are also large over the northern BoB, the sign is opposite to that found in reanalysis (Figure 8c), which is obviously a model bias in capturing the subtropical convection during Indian summer monsoon and the ocean-atmosphere coupled model. The same pattern occurs in WACCM. Since rainfall is not stored in WACCM, the vertical pressure velocities (ω) in the midtroposphere at 500 hPa are used for the correlation analysis. For comparison, the correlations between the CIO mode index and ω at 500 hPa, which are obtained from the NCEPR2 reanalysis, are presented in Figure 8d. Negative (positive) correlations over the BoB (the central Indian Ocean) indicate negative (positive) vertical pressure velocities, that is, updraft (downdraft) over the BoB (the central Indian Ocean), which is consistent with the vertical structure of the CIO mode. In WACCM, there are positive (negative) correlations over the BoB (the central Indian Ocean; Figure 8b), which is opposite to that in the reanalysis (Figure 8d). Thus, in both WACCM and LEN ensembles, during positive CIO mode, there is a weak updraft over the central Indian Ocean and a downdraft occurs over the BoB. Such a vertical structure can be clearly seen from the vertical profiles in Figure 9. Updrafts over the central Indian Ocean are obvious, which, however, do not exist in the reanalysis (see Zhou et al., 2017b).

Overall, using the EOF analysis, it can be concluded that the major mode on intraseasonal timescales in CESM simulations is different from nature, that is, the observed CIO mode. As a result, the force-response relation between the atmosphere and the ocean in the model is nearly opposite to observations. Consistently, the relation between the major mode and MISO in CESM is also opposite to that in observations.

3.4. Evaluation of Simulated CIO Mode: Projection Method

Besides obtaining the CIO mode by applying the EOF analysis with the CESM outputs as discussed above, another way to evaluate the simulated CIO mode is to project the model outputs onto the CIO mode pattern obtained from the observations and reanalysis products. The two ways for extracting the simulated CIO mode provide two different viewpoints for its assessment. As shown in Figure 7, for the first combined EOF mode, the SST mode and low-level zonal wind mode in CESM display an inconsistent structure with that found in nature. For the projection method, the mode patterns are referenced to observations. The extracted oceanic and atmospheric signals maintain a realistic and coherent CIO mode structure (as shown in Figure 7c), which is different from the signals obtained with the former method (as shown in Figures 7a and 7b). The purpose of the projection method is to estimate how much actual CIO mode is involved in each model simulation. Then, one can determine whether energetic simulated CIO mode is favorable for stronger simulated monsoonal rainfall, as it should be in nature. The differences between the two methods are elaborated more in the supporting information. The *x* axis in Figure 10 is the standard deviation (SD) of the projected CIO mode index during the Indian summer monsoon (from June to September), which represents the strength of the CIO mode in a LEN ensemble member. Note that the projected index is

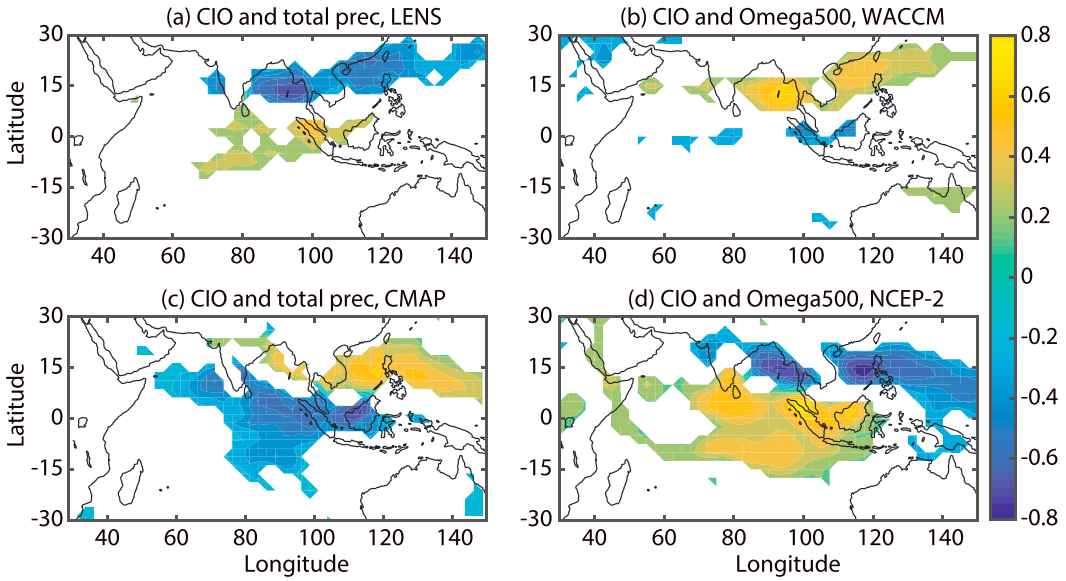

Figure 8. (a) Correlation coefficients between the simulated CIO mode index and precipitation during Indian summer monsoon from June to September in the LEN ensemble #1. (b) Correlation coefficients between the simulated CIO mode index and the intraseasonal ω at 500 hPa during Indian summer monsoon from June to September in WACCM. The simulated CIO mode index is obtained by applying the EOF analysis with model outputs. (c and d) Same as Figures 8a and 8b but calculated with the NCEPR2 reanalysis. All correlation coefficients shown are statistically significant at the 95% confidence level.

dominated by ISVs, and hence, the mean projected index is close to zero and the amplitude of the projected index is represented with its variance. Figure 10a shows the variance of the intraseasonal precipitation anomalies over the northern BoB in the 30 LEN ensembles (10°N–20°N and 85°E–95°E, where the variance of intraseasonal precipitation is large), with respect to the strength of actual CIO mode involved in each ensemble member. The significant correlation coefficient of 0.50 between the variance of intraseasonal precipitation and the projected CIO mode index indicates that a pronounced CIO mode is helpful to reinforce the Indian summer monsoon and to enhance the monsoonal precipitation, which is lacking in the current CESM (Figure 4). The CIO mode controls the propagation direction of tropical ISVs by reinforcing the easterly wind shear over the tropical Indian Ocean and deflecting the tropical ISVs to the north (Zhou et al., 2017b). Such a mechanistic link is confirmed with the LEN ensembles, as shown in Figure 10b. With an increase in the SD of the projected CIO mode index during the Indian summer monsoon, the mean vertical shear of zonal winds (easterly shear is negative) over the tropical Indian Ocean (0–5°N and 70°E–80°E, where the easterly wind shear is enhanced by the CIO mode; Zhou et al., 2017b) becomes stronger. Although the correlation coefficient of −0.38 appears small, it is statistically significant at 95% confidence level. For comparison, the correlation coefficient between the actual CIO mode index and the easterly wind shear in NCEPR2 (also averaged within 0–5°N and 70°E–80°E) during the Indian summer monsoon is −0.22, which is also statistically significant at 95% confidence level. For the LEN ensemble members with a relatively strong CIO mode, the northward propagation of MISO can be clearly seen from the Hovmöller diagram of the composite simulated intraseasonal zonal

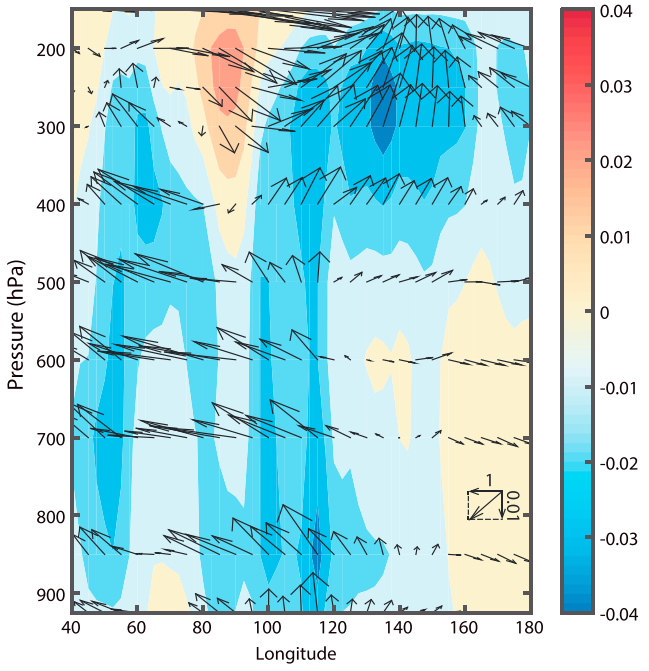

Figure 9. Colors: Differences in the composite intraseasonal ω between the simulated positive and negative CIO mode in WACCM, averaged between 5°N and 5°S. The unit is Pa s^{-1}. Vectors: Differences in the composite intraseasonal zonal and vertical velocities between the simulated positive and negative CIO mode in WACCM, averaged between 5°N and 5°S. The unit for the zonal velocity is m s^{-1}.

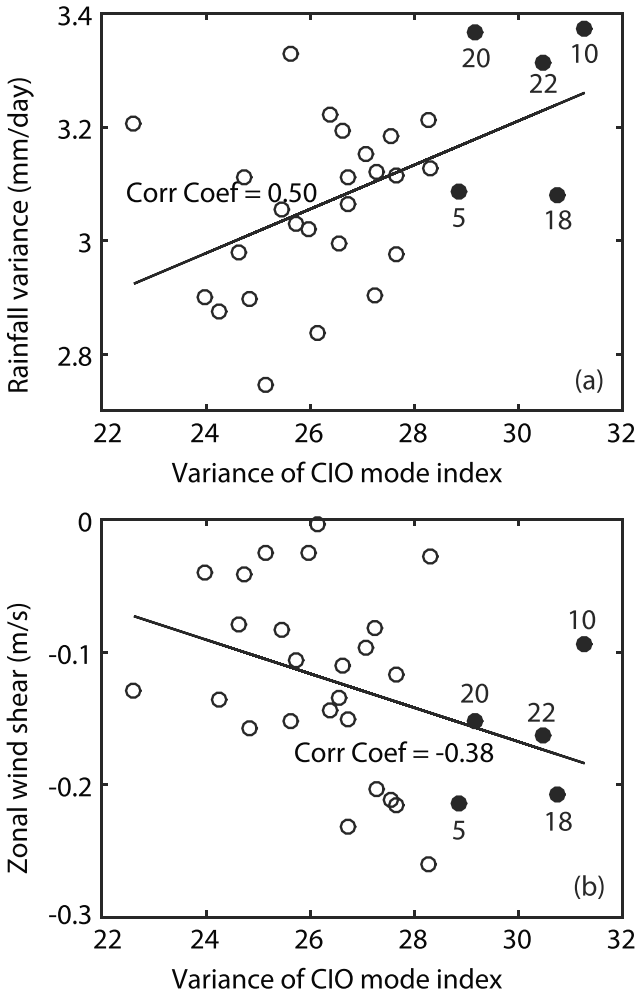

Figure 10. (a) Scatterplots of the variance of the intraseasonal precipitation in the northern BoB (averaged within 10°N–20°N and 85°E–95°E) with respect to the SD of the CIO mode index, which is obtained with the projection method (projecting the model outputs onto the CIO mode obtained with observations and reanalysis products). All results are obtained from the 30 LEN ensembles during the Indian summer monsoon from June to September. The black line is the linear regressions of the scatterplot, and the correlation coefficient is statistically significant at the 95% confidence level. (b) Same as Figure 10a but for the mean vertical shear of intraseasonal zonal winds over the tropical Indian Ocean (averaged within 0–5°N and 70°E–80°E) with respect to the SD of the CIO mode index. The five ensemble members (#5, 10, 18, 20, and 22) that have relatively large variance of projected CIO mode index are represented with filled circles. Note that the variance of projected CIO mode index along the *x* axis represents the relative strength of the actual CIO mode involved in each LEN ensemble member. See the supporting information for more details.

wind anomalies and intraseasonal precipitation (Figure 11a). The corresponding observations and reanalysis are shown in Figure 11c. The negative OLR anomalies obtained from satellite observations are used as the proxy for deep convection. The days when the mean intraseasonal satellite-retrieved OLR anomalies over the tropical Indian Ocean (5°N–10°N and 80°E–90°E, where the large SD of intraseasonal OLR anomalies occur during the Indian summer monsoon) reach a local minimum are selected as the reference days (Day 0) for the composite. Five LEN ensemble members (#5, 10, 18, 20, and 22), which have the largest SD of projected CIO mode index are used to represent the LEN members with a strong simulated CIO mode (Figure 11a; the five ensemble members are represented with filled circles and their ensemble numbers are marked in Figure 10). Northward propagation of simulated intraseasonal winds along with the satellite-retrieved intraseasonal OLR anomalies (Figure 11, white contours) is obvious, and the westerly wind anomalies are to the west of the easterlies, which is consistent with observations. Northward propagation of simulated intraseasonal precipitation (Figure 11, solid contours) is also discernable. However, the intraseasonal precipitation anomalies occur to the west of the westerly wind anomalies. Due to uncertainty in the vertical heating profile, an accurate simulation of the phase relation between precipitation and low-level winds at intraseasonal timescales is still a challenge. In addition, comparing Figures 11a and 11c, one can see that both zonal winds and precipitation in CESM obtained with the projection method are much smaller than the counterparts in nature, which is consistent with the fact that the actual CIO mode in all CESM outputs is very weak and the major modes in all simulations are different from the observed CIO mode (see the supporting information for more detailed explanations). Nevertheless, in comparison with the ensemble mean composite of 30 LEN members (Figure 11b), it can be concluded that a better simulation of the CIO mode is still favorable for the northward propagation of MISO, resulting in stronger Indian summer monsoon and more realistic monsoonal rainfall. Hence, the basic mechanisms still appear to be operational in CESM.

Overall, the projection method tells us how well the actual CIO mode is captured in each LEN ensemble member. Although the observed CIO modes in all members are weak, the members with relatively stronger observed CIO mode can be isolated via the projection method. Then it can be concluded that a better CIO mode is very likely to be favorable for stronger simulations of Indian summer monsoon and MISO in CESM which is consistent with observational evidence for the mechanistic links between CIO and Indian monsoon.

3.5. Simulated CIO Mode and Bias in Large-Scale Circulations

Zhou et al. (2017b) showed that the observed seasonal and interannual variabilities of the CIO mode are mainly attributable to the barotropic energy conversion of the meridional shear of the zonal winds. The simulation of the slow variabilities of the CIO mode is examined by comparing the kinetic energy and its budget terms. According to Zhou, Sobel, et al. (2012), the kinetic energy budget at intraseasonal timescales (KE′) is written as

$$\frac{\partial \mathrm{KE}'}{\partial t} = -\overline{\boldsymbol{U}}\cdot\nabla \mathrm{KE}' + \left[\mathrm{KE}'\times\mathrm{KE}''\right] + \left[\mathrm{KE}'\times\overline{\mathrm{KE}}\right] - \nabla\cdot\left(\boldsymbol{U}'\Phi'\right) + \left[\mathrm{KE}'\times\mathrm{PE}'\right] + \mathrm{EV} + R, \quad (1)$$

where $\mathbf{U} = u\mathbf{i} + v\mathbf{j} + \omega\mathbf{k}$ is the wind vector, Φ is the geopotential, and PE denotes the potential energy. All variables with a bar are for the large-scale background. The variables with a prime denote variabilities at

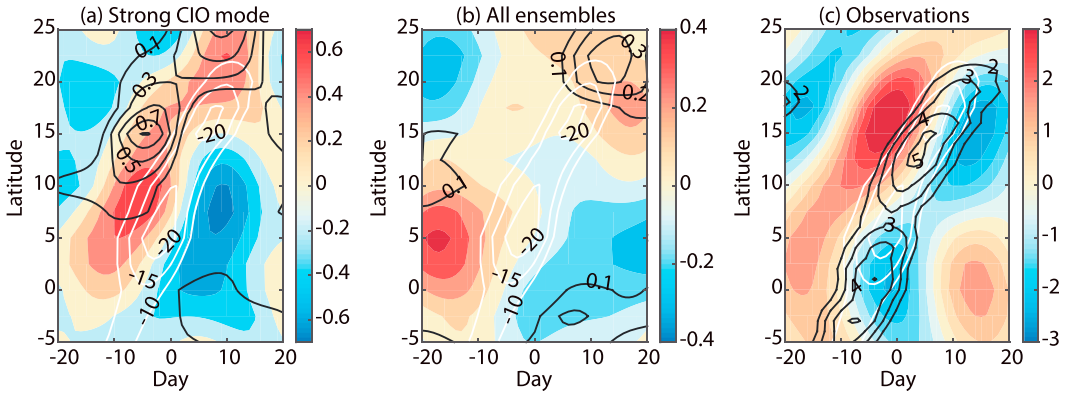

Figure 11. (a) Composite Hovmöller diagram of intraseasonal zonal winds (colors; m s^{-1}), intraseasonal precipitation (solid contours; mm d^{-1}), and the satellite-retrieved intraseasonal OLR anomalies (dashed contours; W m^{-2}), averaged between 80°E and 90°E. The composite is made with five LEN ensemble members (#5, 10, 18, 20, and 22), which have the largest variance of projected CIO mode index (Figure 10). Day 0 is the day when the mean intraseasonal OLR anomalies over the tropical Indian Ocean (5°N–10°N and 80°E–90°E) reach the local minimum during the Indian summer monsoon (from June to September). Negative days are before Day 0 and positive days are after Day 0. (b) Same as Figure 11a but for the composite of 30 LEN members. (c) Same as Figure 11a but for observations and reanalysis. Zonal winds are obtained from the NCEPR2 reanalysis, and precipitation is obtained from CMAP.

intraseasonal timescales, and the variables with double primes are for small scales. $[KE' \times KE'']$ denotes the kinetic energy conversion between the ISVs and the small scale. $\left[KE' \times \overline{KE}\right]$ denotes the kinetic energy conversion between the ISVs and the background. $[KE' \times PE']$ is for the energy conversion between the kinetic energy and the potential energy at intraseasonal timescales. EV is the term for the dot product of the intraseasonal velocity and the zonal eddy component at intraseasonal timescales (see Zhou, Sobel, et al., 2012, for the specific expression), and *R* is the residual term.

In LEN, only winds at several key pressure levels are stored; thus, the following energy calculations are only conducted using the WACCM outputs. The simulated kinetic energy at intraseasonal timescales (obtained with a band-pass filter between 20 days and 100 days and denoted with KE′) is shown in Figure 12a.

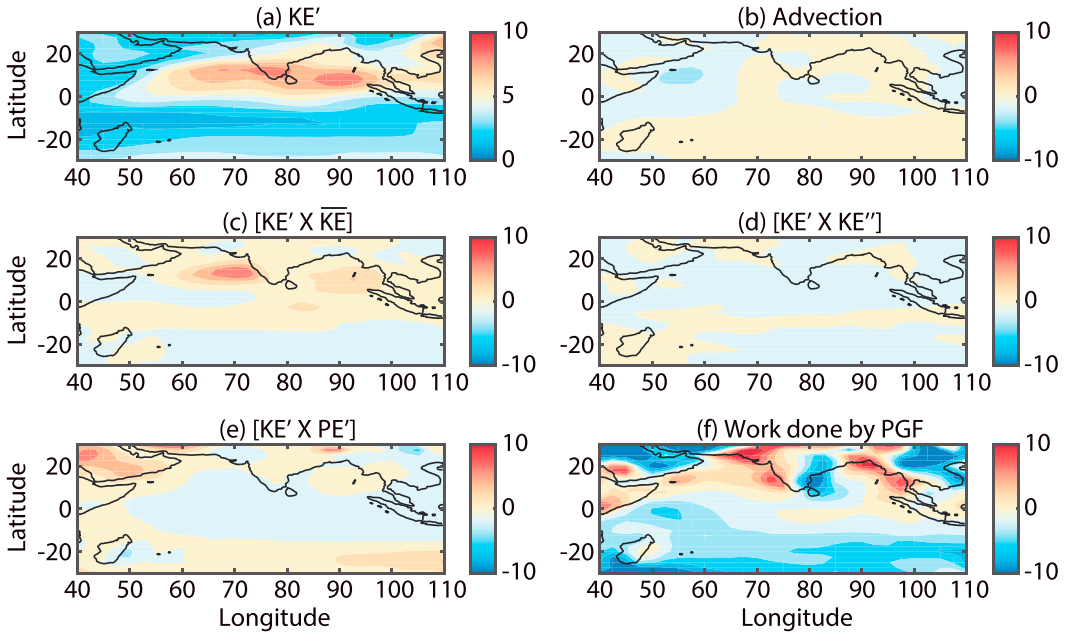

Figure 12. (a) Kinetic energy of ISVs (KE') at 850 hPa in boreal summer, averaged from June to September. The unit for KE' is J kg^{-1}. (b–f) Energy conversion at 850 hPa due to various processes in equation (1) at the intraseasonal timescales, averaged from June to September; Figure 12b is for the advection of KE′, Figure 12c for the energy exchanges between mean KE and KE′, Figure 12d is for the energy exchanges between KE′ and KE at the synoptic scales, Figure 12e for the energy exchanges between the kinetic energy and the potential energy at the intraseasonal timescales, and Figure 12f for the work done by PGF. The unit is J d^{-1} kg^{-1}. All terms are calculated with the WACCM outputs. See Zhou, Sobel, et al. (2012) for more details of the kinetic energy budget.

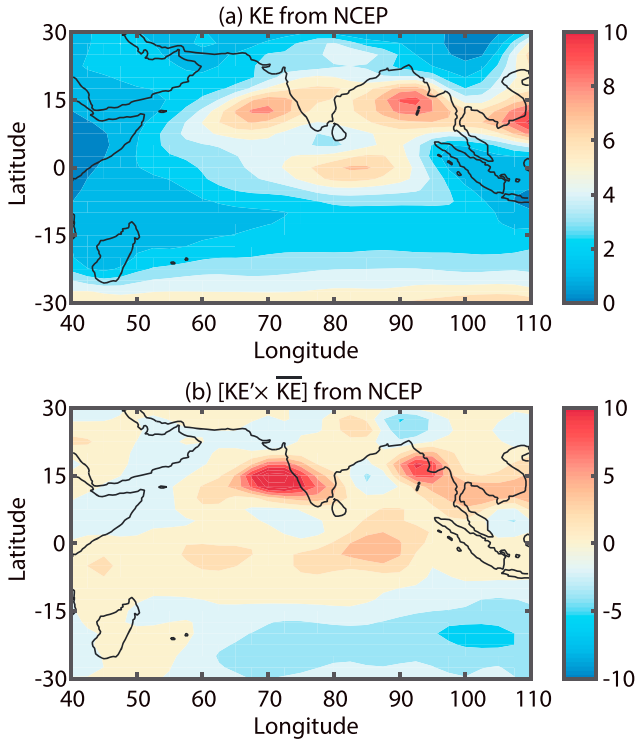

Figure 13. (a) Same as Figure 12a and (b) same as Figure 12c but calculated with the NCEPR2 reanalysis.

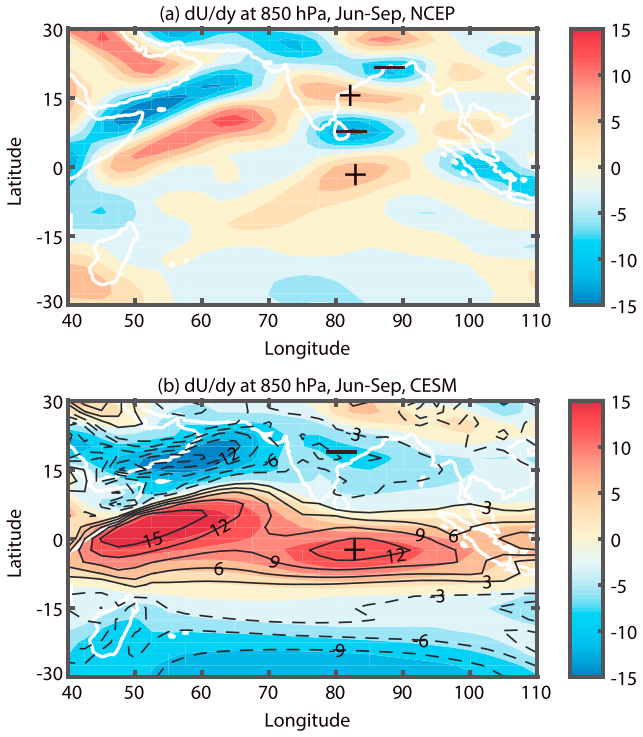

Figure 14. $\partial\overline{u}/\partial y$ at 850 hPa averaged from June to September (a) for the NCEPR2 reanalysis and (b) for the CESM outputs. The unit is m s^{-1} km^{-1}. The plus and minus signs mark the centers of positive and negative $\partial\overline{u}/\partial y$.

Compared with the reanalysis (Figure 13a), large energy values over the Arabian Sea and BoB are reproduced. However, the pronounced KE′ over the central Indian Ocean, corresponding to the CIO mode, is missing. In the reanalysis, the energy of the CIO mode is mainly provided by $\left[KE' \times \overline{KE}\right]$ (the energy transfer from the mean kinetic energy $\overline{KE}$ to the intraseasonal kinetic energy KE′; Figure 13b). However, in CESM, $\left[KE' \times \overline{KE}\right]$ is a moderate energy source to KE′ over the Arabian Sea and BoB (Figure 12c), and the simulated $\left[KE' \times \overline{KE}\right]$ is smaller than it is in the reanalysis. It is slightly positive over the central Indian Ocean and is much weaker than the reanalysis. In CESM, the dominant term in the kinetic energy budget of the CIO mode is the term denoting the work done by the pressure gradient force (PGF; Figure 12f), that is, $-\nabla\cdot\left(\overrightarrow{u'}\Phi'\right)$. This is consistent with the kinetic energy budget of the MJO (Zhou, Sobel, et al., 2012), and it is also consistent with the above conclusion that the MJO is well simulated in the CESM. The small $\left[KE' \times \overline{KE}\right]$ in CESM is attributable to the weak meridional gradient of large-scale zonal winds ($\partial\overline{u}/\partial y$ shown in Figure 14) in simulations. Compared with the NCEPR2 reanalysis, $\partial\overline{u}/\partial y$ at 850 hPa is very similar in CESM except from the central Indian Ocean to BoB. More importantly, the meridional structures of $\partial\overline{u}/\partial y$ in CESM (both WACCM and LEN) and the NCEPR2 reanalysis are different. In NCEPR2 reanalysis, there is a meridional train of positive and negative $\partial\overline{u}/\partial y$, which is critical for satisfying the necessary condition for barotropic instability, i.e., $\beta - \partial^2\overline{u}/\partial y^2$ (where β is the meridional gradient of the Coriolis parameter) changing sign in the study domain. Conversely, in CESM, $\partial\overline{u}/\partial y$ reaches a maximum around the equator (plus symbols) and decreases almost monotonically to its minimum around 20°N (negative symbols). As a result, $\partial^2\overline{u}/\partial y^2$ has the same sign in this region. The $\partial^2\overline{u}/\partial y^2$ in CESM is also too small to overcome β (not shown). Thus, the necessary condition for barotropic instability is not satisfied in CESM and $\left[KE' \times \overline{KE}\right]$ is moderate over the central Indian Ocean, as shown in Figure 12c. Comparing with Figure 2, one can see that although the mean zonal winds are well simulated, the meridional structure of large-scale zonal winds in CESM is actually biased. Such a bias results in the misrepresentation of the CIO mode in CESM. Therefore, the poor simulation of the CIO mode and the MISO are not only attributable to the model deficit at the intraseasonal timescale but also closely related to the bias in the mean state.

4. Conclusions and Discussion

The CIO mode has been recently proposed as a natural mode in the ocean-atmosphere coupled system, and its features at various timescales and its relations to monsoon variability at subseasonal to interannual timescales have been presented in Zhou et al. (2017a, 2017b). In this paper, simulation of the CIO mode in the historical CESM outputs is evaluated. The mean states of low-level winds and SST over the Indo-Pacific region are well simulated in CESM. In addition, the simulated MJO is comparable with observations as also reported in previous studies (e.g., Li et al., 2016; Subramanian et al., 2011). However, the

simulated Indian summer monsoon is weaker than observed and MISO remains a challenge for CESM as highlighted by existing assessments. As an ocean-atmosphere coupled mode, the CIO mode captures the coupled mechanism of MISO. It builds a bridge between the tropics and the subtropics that transfers heat and energy from the equatorial Indian Ocean to the midlatitudes during the Indian summer monsoon. Furthermore, there are clear discrepancies between the observed CIO mode and the CESM simulations. The absence of the CIO mode in CESM simulations (at least partly) explains the weak simulated Indian summer monsoon. The easterly wind anomalies during the positive CIO mode are too strong, and the meridional shear of zonal winds is smaller than reality. As a result of the weak meridional zonal wind shear, according to the WACCM outputs, the kinetic energy transfer from the mean winds to the ISVs is greatly reduced, which cuts off the energy source for MISO in the model. We surmise that the weak $\frac{\partial \overline{u}}{\partial y}$ and associated small barotropic energy conversion may be a critical issue for the poor simulation of the Indian summer monsoon. Although the Indian summer monsoon is generally weak in all CESM outputs, by comparing the 30 LEN ensemble members, one can see that a stronger CIO mode tends to enhance the MISO and improve the Indian summer monsoon simulation (see the supporting information). In addition, the lack of coherence between the ocean-atmosphere interactions also exists with respect to the CIO mode simulation, which was argued to be an essential issue for the poor MISO simulations in various models (Goswami et al., 2014; Meehl et al., 2012). In the reanalysis, an anticyclonic gyre and associated downdraft occur over the warm intraseasonal SST anomalies in the central Indian Ocean, as shown with the reanalysis products in Zhou et al. (2017b). In contrast, in both CESM simulations, warm intraseasonal SST anomalies coexist with a cyclonic gyre and an updraft. Such coexistence is inconsistent with the realistic lead-lag relation between SST anomalies and convection over the Indian Ocean, which is believed to be the critical issue leading to a poor Indian summer monsoon simulation (Fu & Wang, 2004; Vecchi & Harrison, 2002). The ocean-atmosphere interaction in CESM is in fact contrary to observed at intraseasonal timescales, requiring future analysis as to the root causes.

Significant research has addressed the simulation and prediction of Indian summer monsoon, especially the MISO (Abhilash et al., 2014; Lin et al., 2008). Various mechanistic and modeling issues have been examined (e.g., Narapusetty et al., 2016). In this study, CESM shows a persistent deficiency in reproducing the actual CIO mode during the Indian summer monsoon, which can be reasonably assumed to be a fundamental problem in Indian summer monsoon simulations. Since the CIO mode represents the mechanistic link between the dynamic and thermodynamic fields during Indian summer monsoon in the ocean-atmosphere coupled system, the obvious difference of the simulated CIO mode from the reanalysis implies that some intrinsic processes are probably missing in CESM and likely in most current coupled models. Of course, to verify this, the CIO mode simulations in other coupled models need to be systematically assessed. If similar results are obtained, efforts in understanding and improving the CIO mode simulation in modern coupled models will be paramount. A better representation of the CIO mode in a model is expected to improve the phase relation between the oceanic variabilities and the atmospheric circulation, which will in turn contribute to improving the simulation of the Indian summer monsoon and the associated MISO.

In addition, the monsoon system is a critical component in the "seamless" multiscale climate system. The relations between the Indian summer monsoon and major climate modes (such as ENSO and IODZM) are still being debated (Ashok et al., 2001; Gill et al., 2015; Kumar et al., 2006; Sabeerali et al., 2014). The CIO mode, as a climate mode mainly at intraseasonal timescales and with pronounced seasonal and interannual variabilities, provides a new avenue to pinpoint the role of the Indian Ocean and the Indian summer monsoon in the climate system and helps to reveal the relationship between the Indian summer monsoon and other climate processes. Especially considering the monsoon simulations in CESM presented in this study, it is important to understand whether the Walker cell and the local Hadley cell are not properly coupled in climate models. This may hint at the seemingly contradictory claims about the relation between the intraseasonal and interannual variabilities of the Indian summer monsoon (Goswami et al., 2006; Krishnamurthy & Shukla, 2007; Suhas et al., 2012). It can nonetheless be expected that a better reproduction of the CIO mode in a climate model in the future will not only benefit the Indian summer monsoon simulation but also benefit a better simulation of the climate system of the Indian Ocean and South Asia climate as a whole. As a newly proposed natural mode, a comprehensive study on the CIO mode, including its dynamical mechanisms, numerical simulations, and necessary in situ observations, is expected to advance our understanding in the mechanisms of the monsoon system. Our studies this far are but the necessary first steps toward building that comprehensive picture.

Acknowledgments
This work is supported by grants from the National Natural Science Foundation of China (41376034, 41621064, 41690121, and 41690120) and the IPOVAR Project (GASI-IPOVAI-01-02 and GASI-IPOVAI-02). R.M. gratefully acknowledges the CYGNSS grant from NASA and the National Monsoon Mission funds from the Ministry of Earth Sciences (MoES) for partial support. All CESM outputs are obtained from the Earth System Grid (ESG) at http://www.cesm.ucar.edu/. The reanalysis products and observation data for this paper are properly cited and referred to in the reference list.

References

Abhilash, S., Sahai, A. K., Borah, N., Chattopadhyay, R., Joseph, S., Sharmila, S., … Kumar, A. (2014). Prediction and monitoring of monsoon intraseasonal oscillations over Indian monsoon region in an ensemble prediction system using CFSv2. *Climate Dynamics*, *42*(9-10), 2801–2815. https://doi.org/10.1007/s00382-013-2045-9

Ajayamohan, R. S., Khouider, B., & Majda, A. J. (2014). Simulation of monsoon intraseasonal oscillations in a coarse-resolution aquaplanet GCM. *Geophysical Research Letters*, *41*, 5662–5669. https://doi.org/10.1002/2014GL060662

Ashok, K., Guan, Z., & Yamagata, T. (2001). Impact of the Indian Ocean dipole on the relationship between the Indian monsoon rainfall and ENSO. *Geophysical Research Letters*, *28*, 4499–4502.

Boyle, J. S., Klein, S. A., Lucas, D. D., Ma, H. Y., Tannahill, J., & Xie, S. (2015). The parametric sensitivity of CAM5's MJO. *Journal of Geophysical Research: Atmospheres*, *120*, 1424–1444. https://doi.org/10.1002/2014JD022507

Fu, X. H., & Wang, B. (2004). Differences of boreal summer intraseasonal oscillations simulated in an atmosphere–ocean coupled model and an atmosphere-only model. *Journal of Climate*, *17*, 1263–1271.

Fu, X., Wang, B., Waliser, D. E., & Tao, L. (2007). Impact of atmosphere–ocean coupling on the predictability of monsoon intraseasonal oscillations. *Journal of the Atmospheric Sciences*, *64*, 157–174.

Gill, E. C., Rajagopalan, B., & Molnar, P. (2015). Subseasonal variations in spatial signatures of ENSO on the Indian summer monsoon from 1901 to 2009. *Journal of Geophysical Research: Atmospheres*, *120*, 8165–8185. https://doi.org/10.1002/2015JD023184

Goswami, B. N. (2005). South Asian monsoon. In *Intraseasonal variability in the atmosphere–ocean climate system* (pp. 19–61). Berlin: Springer.

Goswami, B. N., & Xavier, P. K. (2005). ENSO control on the south Asian monsoon through the length of the rainy season. *Geophysical Research Letters*, *32*, L18717. https://doi.org/10.1029/2005GL023216

Goswami, B. N., Wu, G., & Yasunari, T. (2006). The annual cycle, intraseasonal oscillations, and roadblock to seasonal predictability of the Asian summer monsoon. *Journal of Climate*, *19*, 5078–5099.

Goswami, B. B., Deshpande, M., Mukhopadhyay, P., Saha, S. K., Rao, S. A., Murthugudde, R., & Goswami, B. N. (2014). Simulation of monsoon intraseasonal variability in NCEP CFSv2 and its role on systematic bias. *Climate Dynamics*, *43*, 2725–2745.

Kanamitsu, M., Ebisuzaki, W., Woollen, J., Yang, S. K., Hnilo, J. J., Fiorino, M., & Potter, G. L. (2002). NCEP-DOE AMIP-II reanalysis (R-2). *Bulletin of the American Meteorological Society*, *83*, 1631–1643.

Kay, J. E., Deser, C., Phillips, A., Mai, A., Hannay, C., Strand, G., … Vertenstein, M. (2015). The Community Earth System Model (CESM) large ensemble project: A community resource for studying climate change in the presence of internal climate variability. *Bulletin of the American Meteorological Society*, *96*(8), 1333–1349. https://doi.org/10.1175/BAMS-D-13-00255.1

Kemball-Cook, S., Wang, B., & Fu, X. H. (2002). Simulation of the intraseasonal oscillation in the ECHAM-4 model: The impact of coupling with an ocean model. *Journal of the Atmospheric Sciences*, *59*, 1433–1453.

Kim, D., Sperber, K., Stern, W., Waliser, D., Kang, I. S., Maloney, E., … Zhang, G. (2009). Application of MJO Simulation Diagnostics to Climate Models. *Journal of Climate*, *22*(23), 6413–6436. https://doi.org/10.1175/2009JCLI3063.1

Kripalani, R. H., & Kumar, P. (2004). Northeast monsoon rainfall variability over south peninsular India vis-à-vis the Indian Ocean dipole mode. *International Journal of Climatology*, *24*, 1267–1282.

Krishnamurthy, V., & Shukla, J. (2007). Intraseasonal and seasonally persisting patterns of Indian monsoon rainfall. *Journal of Climate*, *20*, 3–20.

Kumar, K. K., Rajagopalan, B., Hoerling, M., Bates, G., & Cane, M. (2006). Unraveling the mystery of Indian monsoon failure during El Niño. *Science*, *314*, 115–119.

Lau, W. K. M., Waliser, D. E., & Goswami, B. N. (2012). South Asian monsoon. In *Intraseasonal variability in the atmosphere-ocean climate system* (pp. 21–72). Berlin: Springer.

Li, J., & Zeng, Q. (2002). A unified monsoon index. *Geophysical Research Letters*, *29*, 115–111–115-114.

Li, X., Tang, Y., Zhou, L., Chen, D., Yao, Z., & Islam, S. U. (2016). Assessment of Madden–Julian oscillation simulations with various configurations of CESM. *Climate Dynamics*, *47*, 2667–2690.

Liebmann, B., & Smith, C. A. (1996). Description of a complete (interpolated) outgoing longwave radiation dataset. *Bulletin of the American Meteorological Society*, *77*, 1275–1277.

Lin, J. L., Zhang, M. H., & Mapes, B. (2005). Zonal momentum budget of the Madden-Julian oscillation: The source and strength of equivalent linear damping. *Journal of the Atmospheric Sciences*, *62*, 2172–2188.

Lin, J. L., Kiladis, G. N., Mapes, B. E., Weickmann, K. M., Sperber, K. R., Lin, W., … Scinocca, J. F. (2006). Tropical intraseasonal variability in 14 IPCC AR4 climate models. Part I: Convective signals. *Journal of Climate*, *19*(12), 2665–2690. https://doi.org/10.1175/JCLI3735.1

Lin, J.-L., Weickman, K. M., Kiladis, G. N., Mapes, B. E., Schubert, S. D., Suarez, M. J., … Lee, M. I. (2008). Subseasonal variability associated with Asian summer monsoon simulated by 14 IPCC AR4 coupled GCMs. *Journal of Climate*, *21*(18), 4541–4567. https://doi.org/10.1175/2008JCLI1816.1

Madden, R. A., & Julian, P. R. (1994). Observations of the 40–50-day tropical oscillation—A review. *Monthly Weather Review*, *122*, 814–837.

Marsh, D. R., Mills, M. J., Kinnison, D. E., Lamarque, J.-F., Calvo, N., & Polvani, L. M. (2013). Climate change from 1850 to 2005 simulated in CESM1(WACCM). *Journal of Climate*, *26*, 7372–7391.

McPhaden, M. J., Meyers, G., Ando, K., Masumoto, Y., Murty, V. S. N., Ravichandran, M., … Yu, W. (2009). RAMA: The research moored array for African–Asian–Australian monsoon analysis and prediction*. *Bulletin of the American Meteorological Society*, *90*, 459–480.

Meehl, G. A., Arblaster, J. M., Lawrence, D. M., Seth, A., Schneider, E. K., Kirtman, B. P., & Min, D. (2006). Monsoon regimes in the CCSM3. *Journal of Climate*, *19*, 2482–2495.

Meehl, G. A., Arblaster, J. M., Caron, J. M., Annamalai, H., Jochum, M., Chakraborty, A., & Murtugudde, R. (2012). Monsoon regimes and processes in CCSM4. Part I: The Asian–Australian monsoon. *Journal of Climate*, *25*, 2583–2608.

Murtugudde, R., & Busalacchi, A. J. (1999). Interannual variability of the dynamics and thermodynamics of the tropical Indian Ocean. *Journal of Climate*, *12*, 2300–2326.

Murtugudde, R., McCreary, J. P., & Busalacchi, A. J. (2000). Oceanic processes associated with anomalous events in the Indian Ocean with relevance to 1997–1998. *Journal of Geophysical Research*, *105*, 3295–3306.

Narapusetty, B., Murtugudde, R., Wang, H., & Kumar, A. (2016). Ocean–atmosphere processes driving Indian summer monsoon biases in CFSv2 hindcasts. *Climate Dynamics*, *47*, 1417–1433.

Peña, M., Kalnay, E., & Cai, M. (2003). Statistics of locally coupled ocean and atmosphere intraseasonal anomalies in Reanalysis and AMIP data. *Nonlinear Processes in Geophysics*, *10*, 245–251.

Pottapinjara, V., Girishkumar, M. S., Ravichandran, M., & Murtugudde, R. (2014). Influence of the Atlantic zonal mode on monsoon depressions in the Bay of Bengal during boreal summer. *Journal of Geophysical Research: Atmospheres*, *119*, 6456–6469. https://doi.org/10.1002/2014JD021494

Reynolds, R. W., Smith, T. M., Liu, C., Chelton, D. B., Casey, K. S., & Schlax, M. G. (2007). Daily high-resolution-blended analyses for sea surface temperature. *Journal of Climate*, *20*, 5473–5496.

Sabeerali, C. T., Rao, S. A., George, G., Rao, D. N., Mahapatra, S., Kulkarni, A., & Murtugudde, R. (2014). Modulation of monsoon intraseasonal oscillations in the recent warming period. *Journal of Geophysical Research: Atmospheres*, *119*, 5185–5203. https://doi.org/10.1002/2013JD021261

Slingo, J. M., Sperber, K. R., Boyle, J. S., Ceron, J. P., Dix, M., Dugas, B., … Renno, N. (1996). Intraseasonal oscillations in 15 atmospheric general circulation models: Results from an AMIP diagnostic subproject. *Climate Dynamics*, *12*(5), 325–357. https://doi.org/10.1007/BF00231106

Son, S.-W., Lim, Y., Yoo, C., Hendon, H. H., & Kim, J. (2017). Stratospheric control of the Madden–Julian Oscillation. *Journal of Climate*, *30*, 1909–1922.

Sperber, K. R., & Annamalai, H. (2008). Coupled model simulations of boreal summer intraseasonal (30–50 day) variability, Part 1: Systematic errors and caution on use of metrics. *Climate Dynamics*, *31*, 345–372.

Subramanian, A. C., Jochum, M., Miller, A. J., Murtugudde, R., Neale, R. B., & Waliser, D. E. (2011). The Madden–Julian Oscillation in CCSM4. *Journal of Climate*, *24*, 6261–6282.

Suhas, E., Neena, J. M., & Goswami, B. N. (2012). Interannual variability of Indian summer monsoon arising from interactions between seasonal mean and intraseasonal oscillations. *Journal of the Atmospheric Sciences*, *69*, 1761–1774.

Vecchi, G. A., & Harrison, D. E. (2002). Monsoon breaks and subseasonal sea surface temperature variability in the Bay of Bengal. *Journal of Climate*, *15*, 1485–1493.

Waliser, D. E. (2006). Intraseasonal variability. In *The Asian monsoon* (pp. 203–257). Berlin: Springer.

Waliser, D. E., Jin, K., Kang, I. S., Stern, W. F., Schubert, S. D., Wu, M. L. C., … Park, C. K. (2003). AGCM simulations of intraseasonal variability associated with the Asian summer monsoon. *Climate Dynamics*, *21*(5-6), 423–446. https://doi.org/10.1007/s00382-003-0337-1

Waliser, D. E., Lau, K. M., Stern, W., & Jones, C. (2003). Potential predictability of the Madden-Julian oscillation. *Bulletin of the American Meteorological Society*, *84*, 33–50.

Waliser, D., Sperber, K., Hendon, H., Kim, D., Maloney, E., Wheeler, M., … Woolnough, S. (2009). MJO simulation diagnostics. *Journal of Climate*, *22*, 3006–3030.

Wang, B., & Rui, H. (1990). Synoptic climatology of transient tropical intraseasonal convection anomalies—1975–1985. *Meteorology and Atmospheric Physics*, *44*, 43–61.

Wang, B., Xiang, B., Li, J., Webster, P. J., Rajeevan, M. N., Liu, J., & Ha, K.-J. (2015). Rethinking Indian monsoon rainfall prediction in the context of recent global warming. *Nature Communications*, *6*, 7154. https://doi.org/10.1038/ncomms8154

Weare, B. C., Cagnazzo, C., Fogli, P. G., Manzini, E., & Navarra, A. (2012). Madden-Julian Oscillation in a climate model with a well-resolved stratosphere. *Journal of Geophysical Research*, *117*, D01103. https://doi.org/10.1029/2011JD016247

Webster, P. J., Magana, V. O., Palmer, T. N., Shukla, J., Tomas, R. A., Yanai, M., & Yasunari, T. (1998). Monsoons: Processes, predictability, and the prospects for prediction. *Journal of Geophysical Research*, *103*, 14,451–14,510.

Wheeler, M. C., & Hendon, H. H. (2004). An all-season real-time multivariate MJO index: Development of an index for monitoring and prediction. *Monthly Weather Review*, *132*, 1917–1932.

Wu, G., & Zhang, Y. (1998). Tibetan Plateau forcing and the timing of the monsoon onset over South Asia and the South China Sea. *Monthly Weather Review*, *126*, 913–927.

Xi, J., Zhou, L., Murtugudde, R., & Jiang, L. (2015). Impacts of intraseasonal SST anomalies on precipitation during Indian summer monsoon. *Journal of Climate*, *28*, 4561–4575.

Xie, P., & Arkin, P. A. (1997). Global precipitation: A 17-year monthly analysis based on gauge observations, satellite estimates, and numerical model outputs. *Bulletin of the American Meteorological Society*, *78*, 2539–2558.

Yoneyama, K., Zhang, C., & Long, C. N. (2013). Tracking pulses of the Madden–Julian Oscillation. *Bulletin of the American Meteorological Society*, *94*, 1871–1891.

Zhang, C. D. (2005). Madden-Julian Oscillation. *Reviews of Geophysics*, *43*, RG2003. https://doi.org/10.1029/2004RG000158

Zhou, L., & Murtugudde, R. (2014). Impact of northward-propagating intraseasonal variability on the onset of Indian summer monsoon. *Journal of Climate*, *27*, 126–139.

Zhou, L., Sobel, A. H., & Murtugudde, R. (2012). Kinetic energy budget for the Madden–Julian Oscillation in a multiscale framework. *Journal of Climate*, *25*, 5386–5403.

Zhou, L., Neale, R. B., Jochum, M., & Murtugudde, R. (2012). Improved Madden-Julian Oscillations with improved physics: The impact of modified convection parameterizations. *Journal of Climate*, *25*, 1116–1136.

Zhou, L., Murtugudde, R., Chen, D., & Tang, Y. (2017a). Seasonal and interannual variabilities of the Central Indian Ocean mode. *Journal of Climate*, *30*, 6505–6520.

Zhou, L., Murtugudde, R., Chen, D., & Tang, Y. (2017b). A Central Indian Ocean mode and heavy precipitation during the Indian summer monsoon. *Journal of Climate*, *30*, 2055–2067.